NUCL SCI TECH (2020) 31:62
https://doi.org/10.1007/s41365-020-00769-8

Primary yields of protons measured using CR-39 in laser-induced deuteron–deuteron fusion reactions

Yue Zhang[1,2] · Long-Xiang Liu[1,3] · Hong-Wei Wang[1,2,3] · Yu-Gang Ma[1,2,4] · Bai-Fei Shen[5,6,7] · Guo-Qiang Zhang[1,3] · Mei-Rong Huang[8] · Aldo Bonasera[9,10] · Wen-Peng Wang[5,7] · Jian-Cai Xu[5,7] · Shun Li[5,7] · Gong-Tao Fan[1,3] · Xi-Guang Cao[1,3] · Yong Yu[5] · Jian-Jun He[11] · Chang-Bo Fu[4] · Suyalatu Zhang[8] · Xin-Rong Hu[1,2] · Xin-Xiang Li[1,2] · Zi-Rui Hao[1,2] · Jun-Wen Wang[1,12] · Han Xue[1] · Hai-Juan Fu[1,13]

Received: 7 March 2020 / Revised: 2 April 2020 / Accepted: 7 April 2020 / Published online: 31 May 2020

Abstract Investigating deuteron–deuteron (DD) fusion reactions in a plasma environment similar to the early stages of the Big Bang is an important topic in nuclear astrophysics. In this study, we experimentally investigated such reactions, using eight laser beams with the third harmonic impacting on a deuterated polyethylene target at the ShenGuang-II Upgrade laser facility. This work focused on the application of range-filter (RF) spectrometers, assembled from a 70 μm aluminum filter and two CR-39 nuclear track detectors, to measure the yields of primary DD-protons. Based on the track diameter calibration results of 3 MeV protons used to diagnose the tracks on the RF spectrometers, an approximate primary DD-proton yield of $(8.5 \pm 1.7) \times 10^6$ was obtained, consistent with the yields from similar laser facilities worldwide. This indicates that the RF spectrometer is an effective way to measure primary DD-protons. However, due to the low yields of D^3He-protons and its small track diameter, CR-39 detectors were unable to distinguish it

This work was supported in part by the Strategic Priority Research Program of the Chinese Academy of Sciences (No. XDB160203) and the National Natural Science Foundation of China (Nos. 11875311 and 11421505).

✉ Hong-Wei Wang
wanghongwei@zjlab.org.cn

[1] Shanghai Institute of Applied Physics, CAS, Shanghai 201800, China

[2] University of Chinese Academy of Sciences, Beijing 100049, China

[3] Shanghai Advanced Research Institute, CAS, Shanghai 201210, China

[4] Key Laboratory of Nuclear Physics and Ion-Beam Application (MOE), Institute of Modern Physics, Fudan University, Shanghai 200433, China

[5] State Key Laboratory of High Field Laser Physics, Shanghai Institute of Optics and Fine Mechanics, CAS, Shanghai 201800, China

[6] Department of Physics, Shanghai Normal University, Shanghai 200234, China

[7] CAS Center for Excellence in Ultra-Intense Laser Science, Shanghai 201800, China

[8] College of Physics and Electronics Information, Inner Mongolia University for Nationalities, Tongliao 028000, China

[9] Cyclotron Institute, Texas A&M University, College Station, TX 77843, USA

[10] Laboratori Nazionali del Sud, INFN, Via Santa Sofia, 62, 95123 Catania, Italy

[11] Key Laboratory of Beam Technology of Ministry of Education, College of Nuclear Science and Technology, Beijing Normal University, Beijing 100875, China

[12] ShanghaiTech University, Shanghai 201210, China

[13] Shanghai University, Shanghai 200444, China

from the background spots. Using other accurate detectors may help to measure these rare events.

Keywords Deuteron-deuteron fusion · CR-39 · Range-filter spectrometer · DD-proton

1 Introduction

Nuclear fusion, which is responsible for synthesizing chemical elements and for ensuring stellar equilibrium, is the most crucial reaction in nuclear astrophysics, which is a field that strives for a comprehensive understanding of nuclear reactions in the universe [1–7]. The deuteron–deuteron (DD) fusion reaction, a crucial type of nuclear fusion, plays a key role in aiding the understanding of primordial abundances in Big Bang nucleosynthesis (BBN) models [8] and designing clean nuclear fusion power plants. Therefore, over the past several decades, this reaction has been measured via traditional accelerators in various beam-target experiments [9, 10]. In recent years, with the advent of high-power laser technology, scientists have become particularly interested in investigating these fusion reactions in the plasma environments generated by this new technology, mimicking astrophysical conditions [11–14]. There are two main methods to study fusion reactions: laser direct-driven inertial confinement fusion (ICF) experiments [15–22] and magnetic-confinement fusion experiments [23–25].

In laser-induced nuclear fusion experiments, multiple laser beams release energy onto a small capsule (or a slice containing appropriate fuels) within a short time interval. Subsequently, the target is compressed and heated to reach a high temperature and density, replicating the conditions necessary for a fusion reaction. In addition to neutrons, these reactions produce charged particles such as protons (p), deuterons (D), tritons (T), ^{3}He and alpha particles (α), whose spectral characteristics can reveal specific information concerning the compressed plasma's temperature and density.

For laser-induced DD fusion experiments, the primary fusion reaction equations (1) and (2) are the main fusion channels that occur at the same probability. Considering the high probability of a fusion reaction between T and ^{3}He with D, the energetic primary products may continue to undergo fusion reactions with thermal D in the fuel. These secondary reactions are displayed in Eqs. (3) and (4). Considering only the Q-value of the reaction energy, the 3.5 and 3.6 MeV alpha particles and 14.7 MeV protons are the primary charged products. However, the ^{3}He and T particles produced in the primary reactions have a kinetic energy slightly below 1 MeV, and they may lose further kinetic energy before participating in the secondary reactions through ion collisions in the plasma. As shown in Eqs. (5) and (6), considering both the kinetic energy of the initial particle and the Q-value of the reaction energy, the alpha particle may have an energy of approximately 1.4–6.7 MeV while the proton energy may range from 12.6 to 17.5 MeV. These equations are referred to as the secondary fusion reactions.

Primary reactions:

$$\mathrm{D} + \mathrm{D} \rightarrow n(2.45\,\mathrm{MeV}) + {}^3\mathrm{He}(0.82\,\mathrm{MeV}) \quad 50\%, \tag{1}$$

$$\mathrm{D} + \mathrm{D} \rightarrow p(3.02\,\mathrm{MeV}) + \mathrm{T}(1.01\,\mathrm{MeV}) \quad 50\%. \tag{2}$$

Secondary reactions:

- Considering only the Q-value of the reaction energy,

$$^3\mathrm{He} + \mathrm{D} \rightarrow \alpha(3.6\,\mathrm{MeV}) + p(14.7\,\mathrm{MeV}), \tag{3}$$

$$\mathrm{T} + \mathrm{D} \rightarrow \alpha(3.5\,\mathrm{MeV}) + n(14.1\,\mathrm{MeV}). \tag{4}$$

- Considering the kinetic energy of the initial particle and the Q-value of the reaction energy,

$$^3\mathrm{He}(\leqslant 0.82\,\mathrm{MeV}) + \mathrm{D} \rightarrow \alpha(6.6{-}1.7\,\mathrm{MeV}) + p(12.6{-}17.5\,\mathrm{MeV}), \tag{5}$$

$$\mathrm{T}(\leqslant 1.01\,\mathrm{MeV}) + \mathrm{D} \rightarrow \alpha(6.7{-}1.4\,\mathrm{MeV}) + n(11.9{-}17.2\,\mathrm{MeV}). \tag{6}$$

For such measurements, CR-39 detectors are widely employed to measure protons or other charged particles because they are most sensitive to ions, but insensitive to electrons, X-rays, gamma rays, and electromagnetic noise. Normally, combining CR-39 with a fixed-thickness filter to form a range-filter (RF) assembly, or with a magnet to form a magnet-based charged-particle spectrometer, is used to measure the charged-particle spectra in the laser-plasma experiments [26]. However, when the yields of charged particles are too high, the particle tracks on a magnet-based charged-particle spectrometer will be more likely to overlap. This is a result of the magnets separating different particles, causing the same particles to concentrate in one area. To avoid overlapping tracks, the RF spectrometer assembled from an aluminum film and two CR-39 detectors (see Sect. 3 for details) is employed in this experiment. They measure the fusion products produced by eight laser beams focusing on a flat deuterated polyethylene (CD_2) target, as well as diagnosing the particle types according to the calibrated track diameter results.

In this work, the RF spectrometers were employed to measure primary DD-protons and secondary D^{3}He-protons in laser-induced DD fusion experiments at the ShenGuang-II Upgrade (SG-II-Up) laser facility. Section 2 describes the experimental setup and layout. Section 3 describes the

RF spectrometers used in this experiment and how they were employed to detect protons. Section 4 describes and analyses the results. Finally, concluding remarks and perspectives are written in Sect. 5.

2 Experimental setup and layout

The laser-induced DD fusion reaction was experimentally investigated at the SG-II-Up laser facility at the Shanghai Institute of Optics and Fine Mechanics, Chinese Academy of Sciences. Figure 1a displays the schematic layout of the target chamber, with four laser beams focused on a thin CD_2 target from above and four beams from below. The laser parameters (total energy and pulse duration) ranged from approximately 2 kJ in 250 ps to 19 kJ in 2 ns. The thickness of the CD_2 target varied from 3.6 to 1000 μm, as the laser beam focus varied from 150 to 400 μm. When the eight laser beams focused on the target simultaneously, the impacted area of the target was rapidly compressed and heated to form a surrounding plasma. Subsequently, two ion beams were produced by the lasers interacting with the target, one moving from top to bottom and the other from bottom to top in the plasma. The two beams could collide and create a fusion reaction at the center of the plasma if the kinetic energy of the colliding deuterium ions was sufficient. Here, Faraday cups and Thomson parabolas with image plates were applied to measure the produced ions. Bubble detectors, liquid and plastic scintillators were used to measure the neutrons. A review of the performance of the detectors can be found in Ref. [27].

This work focused on the application and analysis of the RF spectrometers and their results. Figure 1b illustrates a schematic view of the target chamber and locations of the RF spectrometers (A–E), which were used to measure the yields of primary DD-protons and secondary D^3He-protons. The radius of the target chamber was 1.1 m, and the spectrometers were placed between 28 and 85 cm from the target.

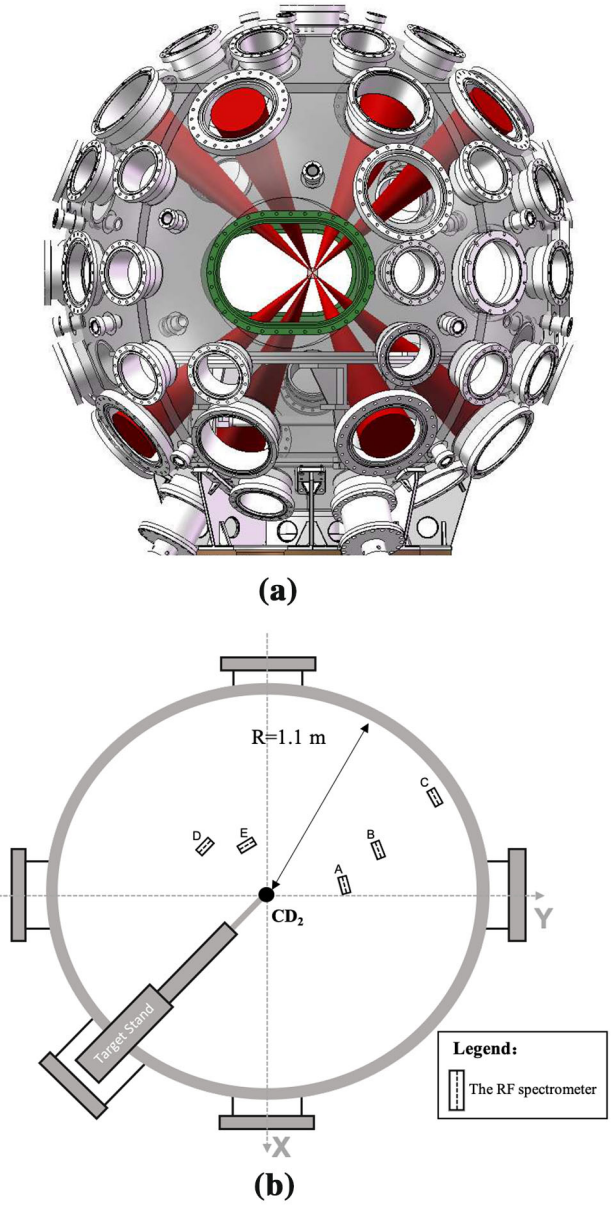

Fig. 1 Experimental setup. **a** Schematic view of the target chamber, with eight laser beams focused on a flat deuterated polyethylene target. **b** Schematic view of the *X*–*Y* plane of the target chamber, with the location of the target, and five RF spectrometers (A–E) highlighted

3 Proton detection with range-filter spectrometer

CR-39, a clear and rigid plastic polymer with the chemical formula $C_{12}H_{18}O_7$, is an ideal material to measure ions in plasma experiments because it is most sensitive to ions but insensitive to electrons, X-rays, gamma rays, and electromagnetic radiation. When ions are incident on a CR-39 sample, they cause damage called a latent track. A latent track can become a micron-scale track, which may be observed by a microscope, after CR-39 is etched in a NaOH solution (see Ref. [28] for more CR-39 track information and growth process). A track's position shows where the ions were incident, and its diameter can often be used to identify the particle type. Track diameters primarily depend on the etch time (t), bulk etch rate (V_B), and track etch rate (V_T), of which the latter two are both sensitive to the normality and temperature of the NaOH solution. Thus, to obtain repeatable results, these factors must be controlled. In this study, the CR-39 samples of size 25 mm (L) × 25 mm (W) × 1.5 mm (H) were manufactured by Track

Analysis Systems Ltd. (TASL) in Bristol, UK. Following the manufacturer's recommendations, an NaOH solution with a molarity of 6.25 mol/L was used because V_T/V_B peaks at concentrations of about 6.25 mol/L for temperatures above 60 °C [29]. Furthermore, a high etch temperature of 98 °C was maintained to reduce the etch time to 1 h, unless otherwise noted. Following the etching process, the track parameters on the CR-39 sample, including the track position, track diameter, and gray level, were recorded by the TASLIMAGE radon dosimetry system, which consists of a computer-based scan system and a charge-coupled device (CCD) camera.

In laser-induced DD fusion experiments, while aiming to detect the number of DD-protons and D^3He-protons with CR-39 detectors, other charged particles such as 0.82 MeV ^3He, 1.4–6.7 MeV alpha particles, and 1.01 MeV T, D, and neutrons should also be considered. For neutrons to leave tracks in a CR-39 detector, they need to generate a moving charged particle via *n–p* scattering or a nuclear reaction with ^{12}C, resulting in a low neutron detection efficiency. Regarding 2.45 MeV and 14.1 MeV neutrons, CR-39's neutron detection efficiency is approximately 10^{-4} counts/neutron [30, 31]. Hence, the tracks left by neutrons can be ignored in comparison with those caused by charged particles.

To prevent proton tracks from mixing with other heavy charged particle tracks, it is necessary to place an appropriately thick aluminum filter in front of the CR-39 to stop the heavy charged particles from reaching the CR-39. In addition, the aluminum filter is used to reduce the proton energy down to around 1 MeV in order to create more visible tracks, as the maximum proton track diameter appears at this energy (see Ref. [26, 32, 33]). According to the charged particle range in aluminum materials shown in Table 1, calculated by the LISE++ program [34, 35], the range of 6.7 MeV alpha particles is 33.1 μm, and the range of 3.02 MeV protons is 81.8 μm. According to the remaining energy listed in Table 1, a 3.02 MeV proton retained 0.86 MeV of energy after passing through 70 μm thick aluminum, which is near the energy of the maximum proton track diameter. However, a 14.7 MeV proton retained 14.12 MeV of energy after passing through the same aluminum filter, which is not in the sensitive energy range of CR-39 for protons (CR-39 is insensitive to the high energy protons above 8 MeV) [26, 36, 37]. Thus, in order to detect these high energy protons, two CR-39 samples are needed. The first serves as an energy degrader, while the later as a track detector.

Based on the above idea, the RF spectrometer assembled from a 70 μm thick aluminum film and two 1.5 mm CR-39 samples (CR-$39^{1\#}$ and CR-$39^{2\#}$) was employed in this study, to measure the DD-protons and D^3He-protons. In the schematic diagram shown in Fig. 2, 1.01 MeV T, 6.7 MeV or lower energy alpha particle, and 0.82 MeV ^3He can be stopped by the 70 μm thick aluminum filter. Meanwhile, the DD-protons reduce their energy passing through the filter, allowing for more efficient proton detection by the CR-$39^{1\#}$ sample. Furthermore, the response of the CR-39 sample covered with a 70-μm-thick aluminum filter for 3 MeV protons was studied with the 2×6 MV tandem accelerator at Peking University's Institute of Heavy Ion Physics. The detailed experimental information can be found in Ref. [36]. After CR-39 tracks were etched for 1 h, the track diameter statistical histogram shown in Fig. 3 was developed. The histogram illustrates that the proton track diameters were distributed between 3 and 8 μm, and the mean proton track diameter was 4.59 μm. These results could be used in the future laser-induced DD fusion experiments to diagnose proton tracks.

Table 1 The charged particle ranges in aluminum material and the remaining energies (RE)

Particle type	Range (μm)[a]	RE_{Al} (MeV)[b]	$RE_{Al+CR-39}$ (MeV)[c]
0.82 MeV ^3He	2.91	0	0
1.01 MeV ^3T	10.09	0	0
6.7 MeV Alpha	33.12	0	0
3.02 MeV Proton	81.81	0.86	0
12.6 MeV Proton	944.04	11.97	0
14.7 MeV Proton	1238.91	14.12	4.90
17.5 MeV Proton	1686.38	16.96	10.05

The table examines the RE of charged particles having passed through an aluminum filter and a CR-39 sample

[a]Charged particle range in aluminum material

[b]RE_{Al} is the remained proton energy after passing through a 70 μm aluminum film

[c]$RE_{Al+CR-39}$ is the remained proton energy after passing through a 70 μm aluminum film and a 1.5 mm CR-39 sample

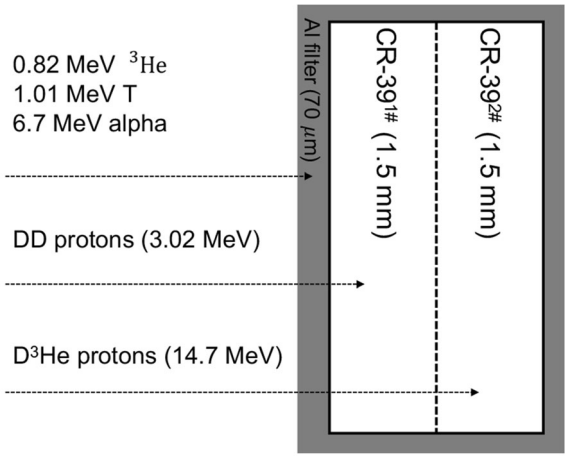

Fig. 2 Schematic diagram of the RF spectrometer assembled from an aluminum film and two CR-39 detectors

discovered on the CR-39$^{1\#}$ sample at position E, while the other four detectors counted fewer tracks. The number of tracks measured by the five detectors at different positions (third column in Table 2) was multiplied by the area of a sphere, with the radius of the detector, to obtain the total yields. As shown in Fig. 7, we concluded that the number of tracks on the CR-39$^{1\#}$ sample at the five positions was approximately consistent with the 4π distribution. A primary DD-proton yield of $(8.5 \pm 1.7) \times 10^6$ was detected via this method for a 210 μm CD_2 target. The results of the other shots at different conditions are shown in Table 3. The primary DD-proton yields were approximately $10^6 - 10^7$, which are consistent with the previous results by similar laser facilities, e.g., Gekko XIII [22] and SG-II [20, 21], but lower than those from OMEGA [26] and the National Ignition Facility [15] which have higher-intensity

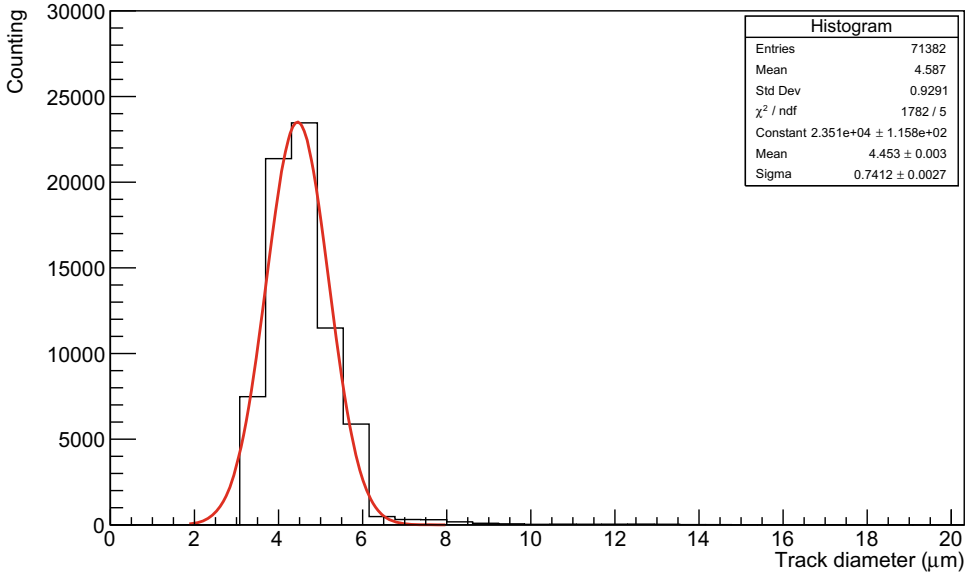

Fig. 3 The histogram of the proton track diameter on a 70 μm aluminum-covered CR-39 sample irradiated by 3 MeV protons. The mean track diameter was 4.587 μm

4 Experimental results

Figure 4a shows the track image detected by the RF spectrometer on the CR-39$^{1\#}$ sample at position E. The tracks were small, consistent with the calibration results (Fig. 4b). Statistical histograms of the five RF spectrometers are shown in Figs. 5 and 6. Figure 5 illustrates the track diameter distribution on the CR-39$^{1\#}$ sample measured by the RF spectrometers, while Fig. 6 displays the results for the CR-39$^{2\#}$ sample. On the CR-39$^{1\#}$ sample, the RF spectrometer closest to the target at position E measured the largest number of tracks; the more distant detectors measured fewer tracks.

Based on the calibration results in Fig. 3, we counted the number of tracks with diameters ranging from 3 to 8 μm in an area of 1 cm × 1 cm (Table 2). Overall, 972 tracks were

laser beams. As Eqs. (1) and (2) have the same reaction probability, the DD-neutron yield should have the same order of magnitude as the DD-proton yield. The presented proton yield is consistent with the DD-neutron yield (10^5–10^8) previously measured by liquid and plastic neutron detectors [27].

Furthermore, there were some tracks recorded at a diameter range of 10–20 μm, whose statistics were similar to those on the CR-39$^{1\#}$ sample at different positions. As heavy ions (such as alpha and T particles and other heavy primary products of DD fusion) are stopped by the 70 μm thick aluminum filter, these tracks might be the primary products at other energy ranges that have not been determined, or the products of primary particles scattered by the aluminum filter. This single type of CR-39 detector had

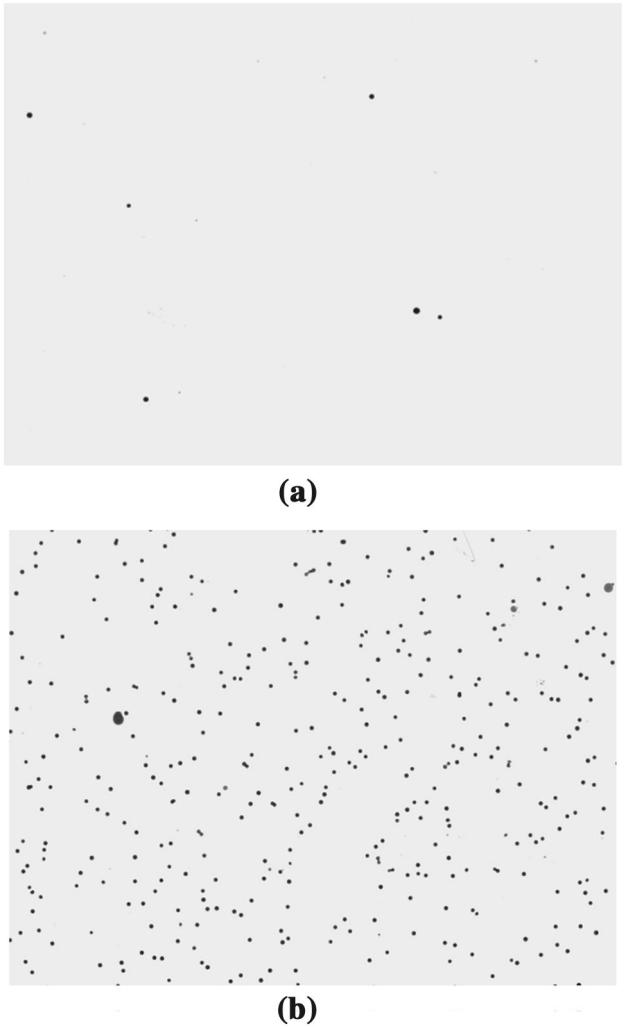

Fig. 4 A digitized microscopic track image (×20 magnification). The physical area of the image is 0.62 mm × 0.46 mm (776 × 582 pixels, where 1 pixel = 0.8 microns). The laser energy in this shot was 13.8 kJ in 2 ns impacting on a 210 μm CD_2 film target. **a** Track image on the CR-39$^{1\#}$ sample from a RF spectrometer. **b** Track image on the CR-39 sample covered with 70 μm aluminum irradiated by 3 MeV protons

difficulty diagnosing their properties; however, a combination of other devices might be able to measure them.

As described in Sect. 3, a 14.7 MeV proton retains 4.90 MeV of energy after passing through a 70 μm thick aluminum filter and a CR-39 sample. According to the proton calibration results in Ref. [36], a 5.0 MeV proton track etched in 98 °C NaOH solution for 1 h does not appear on the CR-39 sample, but has a diameter of around 4 μm after 2 h of etching. However, as shown in Fig. 6, the track diameters on the CR-39$^{2\#}$ sample had a distribution of 3–10 μm, with a few track diameters ranging from 10 to 20 μm. Based on the 5.0 MeV proton calibration results, we conclude that these tracks were not 4.9 MeV proton tracks; they may be proton tracks below 3 MeV, tracks induced by neutrons, or background spots. As CR-39 is insufficient for detecting neutrons, these tracks are more likely to be proton tracks below 3 MeV or background spots. If they were all proton tracks below 3 MeV, the energy of D^3He-protons emitted from the plasma environment should be below 14.7 MeV, and the number of D^3He-proton tracks on the five CR-39$^{2\#}$ samples should meet the 4π distribution requirements. However, the statistical track counts on the CR-39$^{2\#}$ samples are not related to the detector positions shown in the fourth column in Table 2. According to the previous Ref. [26], the D^3He-proton yields are typically three orders of magnitude lower than primary DD-proton yields. Therefore, only three D^3He-protons were expected to be detected in this experiment, easily submerged in the background spots. Thus, these tracks were most likely a mixture of proton tracks below 3 MeV and background spots.

Generally, a proton track is darker than a background spot, but different microscopes (CCD cameras) have different gray-level reading capabilities. Thus, determining the most effective gray value to diagnose a track is very subjective. High gray values may filter the background spots as well as the real signals, so they cannot be effectively used to distinguish the D^3He-proton tracks.

Based on the above analyses, it was difficult to distinguish the secondary D^3He-proton tracks from the background spots based solely on track diameter. Therefore, diagnosing the number of rare D^3He-protons requires more accurate detectors. Silicon carbide (SiC) is one of the most promising wide bandgap materials. Considering previous laser-plasma experiments [38, 39], a SiC detector combined with a magnet that separates low energy charged particles, might be able to measure the number of rare D^3He-protons successfully.

5 Conclusion and perspectives

In the laser-induced primary DD fusion reactions, and secondary D^3He and DT fusion reactions, the yields of charged particles are the basic indicators of an implosion performance. The ratio of the secondary to primary yield is related to the target's areal density. Moreover, when measuring the yields of the charged particle and neutron separately, it is possible to use the values to estimate the target's temperature at burning time.

In this study, according to the calibration results of the 3 MeV proton track diameter on CR-39 covered with 70-μm-thick aluminum, an approximate $(8.5 \pm 1.7) \times 10^6$ primary DD-proton yield was obtained, by employing five RF spectrometers with eight laser beams to induce DD fusion reactions. This shows that the RF spectrometer assembled

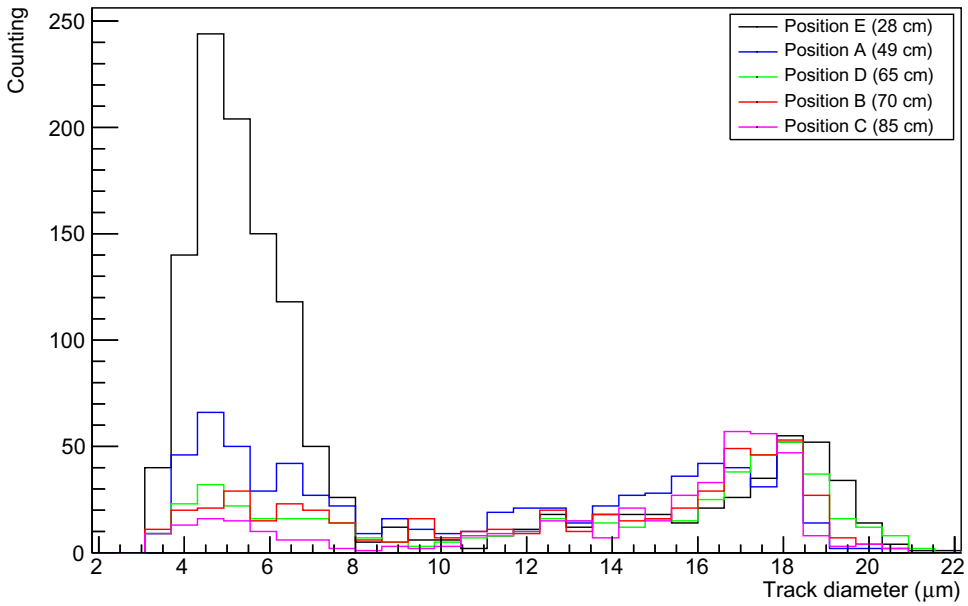

Fig. 5 (Color online) The proton spectra of five RF spectrometers on CR-39[1#]

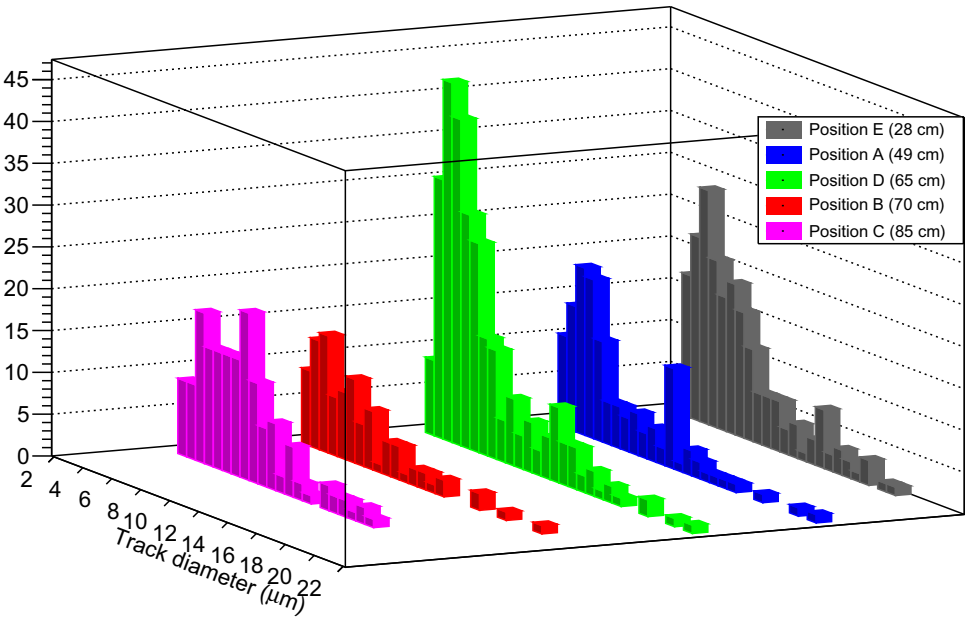

Fig. 6 (Color online) The five proton spectra of five RF spectrometers on CR-39[2#]

Table 2 Statistical results in one shot

RF spectrometer position	Distance (cm)	Counts in CR-39[1#a]	Counts in CR-39[2#a]
E	28 ± 1	972	140
A	49 ± 1	291	87
D	65 ± 1	148	202
B	70 ± 1	153	73
C	85 ± 1	77	112

[a]Counting the track diameters ranging from 3 to 8 μm in one square centimeter area

from fixed-thickness aluminum film and two CR-39 detectors is an effective probe for detecting DD-protons. Furthermore, as the yields of the secondary D^3He-protons were typically lower by three orders of magnitude than those of the primary DD-protons, only three events of D^3He-protons were expected to be detected in this

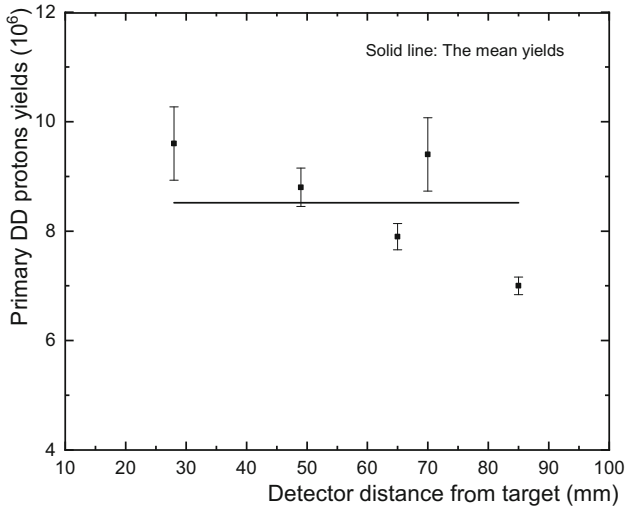

Fig. 7 The primary DD-proton yields detected by five RF spectrometers, with eight lasers impacting on a 210 μm CD_2 target at the SG-II-Up laser facility. The total laser energy is 13.8 kJ in 2 ns

Table 3 Primary DD yield from dense plasmas in different conditions

CD_2 (μm)	Laser energy (kJ)	Duration (ns)	DD proton yields
210	13.8	2.0	$(8.5 \pm 1.7) \times 10^6$
79	14.0	2.0	$(3.0 \pm 1.5) \times 10^6$
79	18.7	3.0	$(1.2 \pm 0.3) \times 10^7$
60[a]	19.3	3.0	$(5.1 \pm 0.9) \times 10^6$
60[a]	19.0	3.0	$(4.2 \pm 0.2) \times 10^6$
60[a]	3.1	0.4	$(2.2 \pm 1.7) \times 10^6$
60[a]	8.0	1.0	$(2.6 \pm 0.8) \times 10^7$
60[a]	13.9	2.0	$(2.8 \pm 1.7) \times 10^7$

[a]The yields of these shots were measured by the RF spectrometer assembled from a 60 μm aluminum and two CR-39 pieces

experiment. Hence, it was difficult to separate D^3He-proton tracks from the background spots in the RF spectrometer.

In general, CR-39 detectors are widely employed to measure charged fusion products when they are energetic enough to escape the plasma. According to the primary DD-proton tracks on the CR-39[1#] sample of the RF spectrometers (associated with the track diameter calibration of CR-39 covered with thick aluminum irradiated by 3 MeV protons), the method described in this research can be used effectively to detect primary DD-protons. In future, to detect D^3He-protons, due to their high energy and low yields, it is necessary to use a suitable filter in front of the CR-39 to reduce the proton energy. Detection could also be achieved by combining magnetic devices to identify the residual energy, which could help separate signals and backgrounds when there are a small number of fusion events.

Acknowledgements The authors would like to thank the engineering staff at the SG-II-Up laser facility for their support, alongside the Engineering Technology Department at the Shanghai Institute of Applied Physics for providing the etching laboratory and CR-39 readout equipment.

References

1. E.M. Burbidge, G.R. Burbidge, W.A. Fowler et al., Synthesis of the elements in stars. Rev. Mod. Phys. **29**, 547–650 (1957). https://doi.org/10.1103/RevModPhys.29.547
2. G. Wallerstein, I. Iben, P. Parker et al., Synthesis of the elements in stars: 40 years of progress. Rev. Mod. Phys. **69**, 995–1084 (1997). https://doi.org/10.1103/RevModPhys.69.995
3. Y.Z. Qian, Neutrinos, supernovae, and the origin of the heavy elements. Sci. China Phys. Mech. Astron. **61**, 049501 (2018). https://doi.org/10.1007/s11433-017-9142-2
4. X.D. Tang, S.B. Ma, X. Fang et al., An efficient method for mapping the $^{12}C+ {}^{12}C$ molecular resonances at low energies. Nucl. Sci. Tech. **30**, 126 (2019). https://doi.org/10.1007/s41365-019-0652-9
5. Z. Li, Z.M. Niu, B.H. Sun, Influence of nuclear physics inputs and astrophysical conditions on *r*-process. Sci. China Phys. Mech. Astron. **62**, 982011 (2019). https://doi.org/10.1007/s11433-018-9355-y
6. S.B. Ma, L.Y. Zhang, J. Hu, Stellar reaction rate of $^{55}Ni(p, \gamma)^{56}Cu$ in type I X-ray bursts. Nucl. Sci. Tech. **30**, 141 (2019). https://doi.org/10.1007/s41365-019-0663-6
7. H.L. Liu, D.D. Han, Y.G. Ma et al., Network structure of thermonuclear reactions in nuclear landscape. Sci. China Phys. Mech. Astron. **63**, 112062 (2020). https://doi.org/10.1007/s11433-020-1552-2
8. R.H. Cyburt, B.D. Fields, K.A. Olive et al., Big bang nucleosynthesis: present status. Rev. Mod. Phys. **88**, 015004 (2016). https://doi.org/10.1103/RevModPhys.88.015004
9. Y. Xu, K. Takahashi, S. Goriely et al., NACRE II: an update of the nacre compilation of charged-particle-induced thermonuclear reaction rates for nuclei with mass number $A < 16$. Nuclear Phys. A **918**, 61–169 (2013). https://doi.org/10.1016/j.nuclphysa.2013.09.007
10. W.J. Li, Y.G. Ma, G.Q. Zhang et al., Yield ratio of neutrons to protons in $^{12}C(d, n)^{13}N$ and $^{12}C(d, p)^{13}C$ from 0.6 to 3 MeV. Nucl. Sci. Tech. (2019). https://doi.org/10.1007/s41365-019-0705-0
11. P. McKenna, K.W.D. Ledingham, T. McCanny et al., Demonstration of fusion–evaporation and direct-interaction nuclear reactions using high-intensity laser–plasma-accelerated ion beams. Phys. Rev. Lett. **91**, 075006 (2003). https://doi.org/10.1103/PhysRevLett.91.075006
12. V.S. Belyaev, A.P. Matafonov, V.I. Vinogradov et al., Observation of neutronless fusion reactions in picosecond laser plasmas. Phys. Rev. E **72**, 026406 (2005). https://doi.org/10.1103/PhysRevE.72.026406
13. L. Robson, P. Simpson, R.J. Clarke et al., Scaling of proton acceleration driven by petawatt–laser–plasma interactions. Nat. Phys. **3**, 58–62 (2007). https://doi.org/10.1038/nphys476
14. L. Torrisi, Nuclear reaction in plasmas generated by high intensity lasers. Radiat. Eff. Defects Solids **172**, 61–73 (2017). https://doi.org/10.1080/10420150.2017.1286657

15. H.S. Park, O.A. Hurricane, D.A. Callahan et al., High-adiabat high-foot inertial confinement fusion implosion experiments on the national ignition facility. Phys. Rev. Lett. **112**, 055001 (2014). https://doi.org/10.1103/PhysRevLett.112.055001
16. D. Lattuada, M. Barbarino, A. Bonasera et al., Model-independent determination of the astrophysical *s* factor in laser-induced fusion plasmas. Phys. Rev. C **93**, 045808 (2016). https://doi.org/10.1103/PhysRevC.93.045808
17. W. Bang, M. Barbui, A. Bonasera et al., Temperature measurements of fusion plasmas produced by petawatt–laser-irradiated D_2–^{3}He or CD_4–^{3}He clustering gases. Phys. Rev. Lett. **111**, 055002 (2013). https://doi.org/10.1103/PhysRevLett.111.055002
18. R. Betti, O. Hurricane, Inertial-confinement fusion with lasers. Nat. Phys. **12**, 435–448 (2016). https://doi.org/10.1038/nphys3736
19. R.S. Craxton, K.S. Anderson, T.R. Boehly et al., Direct-drive inertial confinement fusion: a review. Phys. Plasmas **22**, 110501 (2015). https://doi.org/10.1063/1.4934714
20. X.P. Zhang, J.R. Zhao, D.W. Yuan et al., Deuteron–deuteron fusion in laser-driven counter-streaming collisionless plasmas. Phys. Rev. C **96**, 055801 (2017). https://doi.org/10.1103/PhysRevC.96.055801
21. J.R. Zhao, X.P. Zhang, D.W. Yuan et al., Neutron yield enhancement in laser-induced deuterium–deuterium fusion using a novel shaped target. Rev. Sci. Instrum. **86**, 063505 (2015). https://doi.org/10.1063/1.4922912
22. R. Kodama, P. Norreys, K. Mima et al., Fast heating of ultra high-density plasma as a step towards laser fusion ignition. Nature **412**, 798–802 (2001). https://doi.org/10.1038/35090525
23. E. Ghorbanpour, A. Ghasemizad, S. Khoshbinfar, Non-equilibrium ignition criterion for magnetized deuterium–tritium fuel. Nucl. Sci. Tech. **30**, 67 (2019). https://doi.org/10.1007/s41365-019-0592-4
24. J. Ongena, R. Koch, R. Wolf et al., Magnetic-confinement fusion. Nat. Phys. **12**, 398–410 (2016). https://doi.org/10.1038/nphys3745
25. R. Betti, P.Y. Chang, B.K. Spears et al., Thermonuclear ignition in inertial confinement fusion and comparison with magnetic confinement. Phys. Plasmas **17**, 058102 (2010). https://doi.org/10.1063/1.3380857
26. F.H. Séguin, J.A. Frenje, C.K. Li et al., Spectrometry of charged particles from inertial-confinement-fusion plasmas. Rev. Sci. Instrum. **74**, 975–995 (2003). https://doi.org/10.1063/1.1518141
27. G. Zhang, M. Huang, A. Bonasera et al., Nuclear probes of an out-of-equilibrium plasma at the highest compression. Phys. Lett. A **383**, 2285–2289 (2019). https://doi.org/10.1016/j.physleta.2019.04.048
28. D. Nikezic, K. Yu, Formation and growth of tracks in nuclear track materials. Mater. Sci. Eng. R Rep. **46**, 51–123 (2004). https://doi.org/10.1016/j.mser.2004.07.003
29. J. Charvát, F. Spurný, Optimization of etching characteristics for cellulose nitrate and CR-39 track detectors. Int. J. Radiat. Appl. Instrum. Part D Nuclear Tracks Radiat. Meas. **14**, 447–449 (1988). https://doi.org/10.1016/1359-0189(88)90003-9
30. J.A. Frenje, C.K. Li, F.H. Séguin et al., Absolute measurements of neutron yields from DD and DT implosions at the OMEGA laser facility using CR-39 track detectors. Rev. Sci. Instrum. **73**, 2597–2605 (2002). https://doi.org/10.1063/1.1487889
31. S. Cavallaro, Note: fast neutron efficiency in CR-39 nuclear track detectors. Rev. Sci. Instrum. **86**, 036103 (2015). https://doi.org/10.1063/1.4915502
32. Y.F. He, X.F. Xi, S.L. Guo et al., Calibration of CR-39 solid state track detectors for study of laser driven nuclear reaction. Nucl. Sci. Tech. **31**, 42 (2020). https://doi.org/10.1007/s41365-020-0749-1
33. M. Seimetz, P. Bellido, P. García et al., Spectral characterization of laser-accelerated protons with CR-39 nuclear track detector. Rev. Sci. Instrum. **89**, 023302 (2018). https://doi.org/10.1063/1.5009587
34. O. Tarasov, D. Bazin, LISE++: radioactive beam production with in-flight separators. Nuclear Instrum. Methods Phys. Res. Sect. B Beam Interact. Mater. Atoms **266**, 4657–4664 (2008). https://doi.org/10.1016/j.nimb.2008.05.110
35. O. Tarasov, D. Bazin, LISE++: design your own spectrometer. Nuclear Phys. A **746**, 411–414 (2004). https://doi.org/10.1016/j.nuclphysa.2004.09.063
36. Y. Zhang, H.W. Wang, Y.G. Ma et al., Energy calibration of a CR-39 nuclear-track detector irradiated by charged particles. Nucl. Sci. Tech. **30**, 87 (2019). https://doi.org/10.1007/s41365-019-0619-x
37. N. Sinenian, M.J. Rosenberg, M. Manuel et al., The response of CR-39 nuclear track detector to 1–9 MeV protons. Rev. Sci. Instrum. **82**, 103303 (2011). https://doi.org/10.1063/1.3653549
38. M. Cutroneo, P. Musumeci, M. Zimbone et al., High performance SiC detectors for MeV ion beams generated by intense pulsed laser plasmas. J. Mater. Res. **28**, 87–93 (2013). https://doi.org/10.1557/jmr.2012.211
39. H.J. Fu, L.J. Wang, H.W. Wang et al., The R&D of 4H–SiC detector for laser plasma products measurement. Nucl. Tech. **42**, 020501 (2019). https://doi.org/10.11889/j.0253-3219.2019.hjs.42.020501